Strato-mesospheric ozone measurements using ground-based millimeter-wave spectroscopy at Thule, Greenland

Giovanni Muscari,[1] Claudio Cesaroni,[1] Irene Fiorucci,[1] Anne K. Smith,[2] Lucien Froidevaux,[3] and Martin G. Mlynczak[4]

Received 13 September 2011; revised 28 February 2012; accepted 4 March 2012; published 13 April 2012.

[1] On January 2009 a ground-based millimeter-wave spectrometer (GBMS) was installed at Thule Air Base (76.5°N, 68.8°W), Greenland, for long-term winter monitoring of several stratospheric and mesospheric trace gases in the framework of the Network for the Detection of Atmospheric Composition Change. This work is aimed at characterizing the GBMS O_3 vertical profiles between 35 and 80 km altitude obtained by applying the optimal estimation method to O_3 pressure-broadened spectral line measurements carried out during three winters. In this altitude range, GBMS O_3 retrievals are highly sensitive to variations of the atmospheric state, and their accuracy is estimated to be the larger of 11% or 0.2 ppmv. Comparisons of GBMS O_3 profiles with colocated satellite-based measurements from Aura Microwave Limb Sounder (MLS) and Thermosphere Ionosphere Mesosphere Energetics and Dynamics Sounding of the Atmosphere using Broadband Emission Radiometry (SABER) show a good agreement below 65 km altitude once the known 10%–20% high bias of SABER O_3 profiles is considered, with the GBMS displaying an averaged low bias of ∼9% and 17% with respect to MLS and SABER. In the nighttime mesosphere, the GBMS detects the ozone tertiary maximum within 0.1 ppmv (6%) on average with respect to the convolved MLS, SABER, and global 3-D ROSE model profiles but shifts its position to lower altitudes by 4–5 km compared to the height obtained by the other three data sets. In the 50–80 km altitude range, estimates of mesospheric O_3 diurnal variation obtained from the GBMS and the convolved satellite measurements agree well within the ±1 standard deviation (∼0.6 ppmv) of the GBMS mean profile.

Citation: Muscari, G., C. Cesaroni, I. Fiorucci, A. K. Smith, L. Froidevaux, and M. G. Mlynczak (2012), Strato-mesospheric ozone measurements using ground-based millimeter-wave spectroscopy at Thule, Greenland, *J. Geophys. Res.*, *117*, D07307, doi:10.1029/2011JD016863.

1. Introduction

[2] Winter measurements of stratospheric and mesospheric constituents have been regularly carried out since January 2009 from the Network for the Detection of Atmospheric Composition Change (NDACC) station at Thule Air Base (76.5°N, 68.8°W), Greenland, by means of a ground-based millimeter-wave spectrometer (GBMS) designed and built at the State University of New York at Stony Brook [*de Zafra*, 1995; *Di Biagio et al.*, 2010, and references therein]. The GBMS measures rotational emission spectra of atmospheric chemical species such as O_3, N_2O, CO, and HNO_3, as well as the H_2O continuum, with a spectral window of 600 MHz tunable between approximately 230 and 280 GHz. By means of the observed line shape, together with pressure and temperature vertical profiles, a mathematical deconvolution process exploits the pressure broadening of spectral lines to determine the emitting molecule's concentration as a function of altitude from about 15 to 80 km. For water vapor, only the integrated column density can be obtained [*Fiorucci et al.*, 2008].

[3] In this work we discuss the upper stratospheric and mesospheric GBMS O_3 profiles obtained at Thule by deconvolving the pressure-broadened emission lines at 264.925 and 276.923 GHz. These measurements were never before compared with colocated data sets or model results. In the past, the GBMS spectra were processed using the Chahine-Twomey deconvolution technique [e.g., *Cheng et al.*, 1996] or an iterative matrix inversion method employing a vertical smoothing constraint [*de Zafra et al.*, 1997; *Muscari et al.*, 2007]. Both methods are illustrated in the work of *Twomey* [1977]. More recently, we updated the retrieval algorithm used for inverting all the observed species adapting the optimal estimation (OE) method [*Rodgers*,

[1]Istituto Nazionale di Geofisica e Vulcanologia, Rome, Italy.
[2]Atmospheric Chemistry Division, National Center for Atmospheric Research, Boulder, Colorado, USA.
[3]Jet Propulsion Laboratory, California Institute of Technology, Pasadena, California, USA.
[4]NASA Langley Research Center, Hampton, Virginia, USA.

0148-0227/12/2011JD016863

1976, 2000; *Connor et al.*, 1995] to GBMS spectral data (for the application to the HNO_3 data set, see *Fiorucci et al.* [2011]). This effort is aimed at conforming GBMS retrievals to the standard of the NDACC microwave group, and providing our retrievals with a set of averaging kernels that allow more straightforward comparisons with other data sets.

[4] Ozone plays a fundamental role in the chemical and radiative processes of the middle atmosphere. In the mesosphere, the ozone budget is regulated almost entirely by the absorption of ultraviolet radiation by O_2 and O_3 (between 137 and 300 nm, in the Herzberg continuum, the Schumann-Runge bands and continuum, and the Hartley band), and by odd hydrogen ($HO_x = H^+OH^+HO_2$) catalytic cycles [e.g., *Brasseur and Solomon*, 2005]. Above the stratopause, the ozone photochemical lifetime is short and photochemistry prevails over transport as the main process regulating ozone concentrations. In particular, at Northern Polar latitudes, as the Sun rises just above the horizon, mesospheric O_3 vertical profiles shift from typical nighttime to daytime distributions in one and a half hours or less. During the long Polar winter nights, however, O_3 is not necessarily in photochemical equilibrium in the upper stratosphere/mesosphere and the intense dynamics that characterize those regions can determine ozone concentrations. A peculiar feature of high-latitude mesospheric O_3 mixing ratio (vmr) vertical profiles is the so-called tertiary ozone maximum, which has been detected by satellite- and ground-based instruments and explained by means of modeling efforts [e.g., *Froidevaux et al.*, 1996; *Marsh et al.*, 2001; *Hartogh et al.*, 2004].

[5] Although there are about 70 NDACC stations over the globe and many of them provide stratospheric ozone measurements, at polar latitudes there are only two sites, Thule and Ny Alesund (both in the Arctic), that are capable of providing O_3 mixing ratio vertical profiles above 55 km. Information on mesospheric O_3 concentrations at high latitudes is therefore scarce, especially with respect to variations that occur on time scales difficult to investigate using satellite-based instruments (long-term, i.e., more than a few years, or short-term, i.e., less than a few hours). In contrast to this limited coverage, accurate ground-based O_3 measurements, and measurements of diurnal ozone variations in particular, can provide important observational constraints to the photochemistry and dynamics of atmospheric 3-D models, especially at polar latitudes where atmospheric parameters can reach unparalleled values. Reliable global atmospheric models, in turn, are essential toward improving our understanding of middle atmospheric processes and are a necessary tool for studies on ozone recovery and climate changing scenarios. Additionally, consistent long-term ground-based measurements are a unique tool for bridging between global satellite-based measurements, either by cross-calibrating them or by filling gaps in temporal coverage.

[6] This work will illustrate the main characteristics of the GBMS mesospheric O_3 retrievals from Thule, presenting the adaptation of the OE method to GBMS O_3 spectra. In order to evaluate the quality of this data set, we compared GBMS O_3 retrievals from 35 to 80 km altitude with coincident measurements from the NASA Aura Microwave Limb Sounder (MLS) instrument [*Waters et al.*, 2006; *Froidevaux et al.*, 2008], from the Sounding of the Atmosphere using Broadband Emission Radiometry (SABER) instrument on board the Thermosphere Ionosphere Mesosphere Energetics and Dynamics (TIMED) satellite [*Russell et al.*, 1999; *Rong et al.*, 2009], and with results from ROSE, a global three-dimensional mechanistic chemical dynamical model [*Smith and Marsh*, 2005, and references therein].

2. GBMS Instrumental Setup

[7] The GBMS observes millimeter-wave signals (230–280 GHz range) arising from molecular rotational transitions. It employs the power balancing technique, with a rotating reflective semicircular chopper wheel switching with ~1 Hz frequency from the reference beam pointing in the zenith direction to the signal beam pointing between 10° and 15° above the horizon. A dielectric sheet placed in the reference beam compensates for the lower total power received from atmospheric emission near the zenith, while a servo mechanism continuously adjusts the signal beam angle as atmospheric opacity changes, seeking to maintain power balance in the two beams.

[8] After the signal is down-converted in frequency and amplified, intensity versus frequency spectra are produced by means of two Acousto-Optical Spectrometers (AOSs). One AOS (wide band) has a total spectral range of 600 MHz (that can be tuned anywhere between 230 and 280 GHz) and a resolution of ~1.2 MHz/channel, while the second AOS (narrow band) has a spectral window of 50 MHz tunable within the range of the wide-band AOS, and a resolution of ~65 kHz/channel. Taking advantage of the dependence of the emission line broadening on atmospheric pressure, deconvolution algorithms allow the retrieval of mixing ratio vertical profiles for the observed trace gases. In particular, the combination of the wideband and narrowband spectrometers allows the retrieval of vertical profiles of atmospheric constituents from approximately 15 to 80 km altitude with a vertical resolution ranging from 10 to 12 km (see section 3). At the observed frequencies, however, molecular emissions from above ~60 km generate a line pressure broadening which gradually (with increasing altitude) loses importance with respect to the Doppler broadening (which depends on frequency and temperature, not on pressure). The vertical resolution of GBMS O_3 vertical profiles therefore degrades rapidly starting at ~65 km altitudes (see section 3).

[9] The GBMS measurements employed in this study are obtained observing the pure rotational transition lines of O_3 at 276.923 GHz or 264.926 GHz using only the narrowband AOS. Moreover, since we focus here on the upper stratospheric/mesospheric O_3, the profiles discussed encompass only the 35–80 km vertical region. All the spectral information needed to deconvolve the O_3 lines are obtained from the Jet Propulsion Laboratory (JPL) spectral catalog (available at http://spec.jpl.nasa.gov) [*Pickett et al.*, 1998], except for the pressure broadening coefficients (2.330 MHz/hPa and 2.497 MHz/hPa for the 276.923 GHz and 264.926 GHz lines, respectively) and their temperature dependence coefficient ($n = -0.77$) which are obtained from the HITRAN 2008 database (http://www.cfa.harvard.edu/hitran) [*Rothman et al.*, 2009]. Spectra are saved in 15 min integration time bins, and then, when necessary in order to improve the signal-to-noise ratio, they are further integrated in longer time bins during data processing. When this occurs, the 15 min spectra to be averaged together are first compared with one another to ensure

that potential differences from spectrum to spectrum are well within their noise level. During GBMS observations at Thule, the atmospheric opacity ranged between 0.1 and 0.3 Nepers at 270 GHz and ground temperatures generally stayed between −15 and −30°C. Further information on the observing technique and the equations which govern it are given by *Parrish et al.* [1988], *de Zafra* [1995], and *Fiorucci et al.* [2008].

3. The GBMS O_3 Data Set

[10] The GBMS O_3 measurements used in this study have been obtained during the three winter campaigns carried out at Thule during the first two or three months of 2009, 2010, and 2011. As mentioned in the Introduction, the inversion algorithm applied to all GBMS observed spectra (O_3, HNO_3, CO, and N_2O) has recently been changed to the optimal estimation technique. *Fiorucci et al.* [2011] provide all the details of this implementation and illustrate how this change affected the existing GBMS HNO_3 data set. Extensive tests aimed at evaluating how the change in retrieval algorithm affected previously published GBMS data have also been carried out for O_3 spectra. Results (unpublished, 2010) show an agreement between OE O_3 retrievals and previous analyses better than the larger of 5% or 0.2 ppmv at all altitudes. Here we will discuss only those aspects of the OE retrieval technique that are unique to the GBMS O_3 spectra involved in this study. We redirect the reader to the work of *Fiorucci et al.* [2011] and to many other discussions on the OE method present in the literature [e.g., *Connor et al.*, 1995; *Nedoluha et al.*, 1995; *Coe et al.*, 2002] for all the standard equations (involved in the forward modeling, the a priori contribution, the covariance matrices and retrieval error characterization) essential to the application of this algorithm.

[11] In implementing the OE, the values attributed to the variances σ_a^2 and σ_ε^2 (diagonal elements of the covariance matrices of a priori profile and measured spectrum, respectively) determine the contribution of the a priori profile and of the spectral measurement to the retrieval. Very small errors in the a priori profile strongly constrain the retrieved profile to the a priori information, while large σ_a values (or small σ_ε) lead to solutions relying mostly on the spectral measurement and with a tendency to oscillate when σ_a is too large (or σ_ε too small) for the noise level of the spectrum. For the analysis of GBMS data sets, both covariance matrices are treated as adjustable parameters whose values are set empirically by optimizing the performance of the retrieval process in order to have the best possible resolution without introducing ambiguous oscillations in the solutions [*Parrish et al.*, 1992; *Fiorucci et al.*, 2011]. The parameter σ_ε is held fixed across the spectrum, whereas the error on the a priori, σ_a, is set to vary with altitude. Additionally, *Fiorucci et al.* [2011] show that increasing measurement errors or decreasing a priori uncertainties by the same factor leads to analogous solution profiles and only the relative weight of the two matrices, not the absolute value of their elements, affects the retrieved profile.

[12] Ultimately, since the noise level of GBMS spectra used in this study does not vary significantly from spectrum to spectrum, we use the same σ_ε value to invert all GBMS spectra. Conversely, since mesospheric O_3 concentrations are much more variable and unpredictable during nighttime than during sunlit hours, two separate σ_a profiles for nighttime and daytime spectra (that differ only at mesospheric altitudes) are employed. In Figure 1, analysis results for the nighttime measurement of 22 February 2011 are presented. The measured spectrum and the corresponding OE generated spectrum (almost perfectly matching and therefore hardly visible as separate lines) are depicted in Figure 1d, their difference is drawn in Figure 1e, the a priori and retrieved profiles are shown in Figure 1a (dashed and solid lines, respectively), and uncertainties associated with the retrieved profile (see later discussion) are presented in Figure 1b. Although the a priori O_3 vmr profile shown in Figure 1a (for the most part taken from the climatology of early winter at high latitudes) is used for nighttime measurements only, it is identical to the daytime a priori in the altitude range of interest, that is, below 80 km altitude. The two profiles differ only in the magnitude of the mesopause O_3 vmr peak at 92 km which is set at 6 ppmv during nighttime and 1 ppmv during daytime. Furthermore, the specific a priori used for retrieving GBMS profiles does not affect the comparison with higher vertical resolution correlative data sets if the latter are convolved using the averaging kernels and the a priori adopted for the GBMS data analysis. Figures 1f and 1c show the averaging kernels (AKs) and their full width at half maximum (FWHM), respectively, with the latter used as an indication of the vertical resolution of the retrieval up to approximately 60–65 km. Upward of this altitude range, Doppler prevails over pressure broadening and the AKs start to display important secondary peaks leading to FWHM values that are not a meaningful representation of the vertical resolution [*Connor et al.*, 1995]. It is worth pointing out, however, that numerous tests have shown that the inversion technique locates maxima of the O_3 mixing ratio vertical profile (as well as that of other species) with an accuracy that is better than what the FWHM value at the altitude of a mixing ratio maximum would indicate. Empirically, we find that such an accuracy is well represented by the distance between the peak altitude of a AK curve and the nominal altitude for which the same AK is calculated.

[13] Each AK represents the sensitivity of the retrieval at a given altitude to variations in O_3 at all altitudes. If the area under each AK curve (dashed black line in Figure 1f, hereinafter referred to as "sensitivity") is close to unity then the retrieval at that altitude is sensitive to variations of the atmospheric state. For this reason, GBMS O_3 vmr profiles discussed in this work should be considered for scientific studies only at altitudes where the sensitivity is $\sim 1.0 \pm 0.2$, and Figure 1f suggests that this condition is fulfilled in the altitude range 31–80 km. However, we confine the presented intercomparison upward of 35 km because a separate set of GBMS observations, obtained using the wideband AOS (see section 2), are better suited for studying the lower stratosphere and will be discussed in a future publication.

[14] The uncertainties in the retrieved GBMS O_3 profiles (see Figure 1b) are due to different sources: instrument calibration, data scaling, forward model parameters, measurements noise and smoothing errors. Those related to the calibration and data scaling procedures (e.g., errors in receiver temperature and atmospheric opacity) are estimated

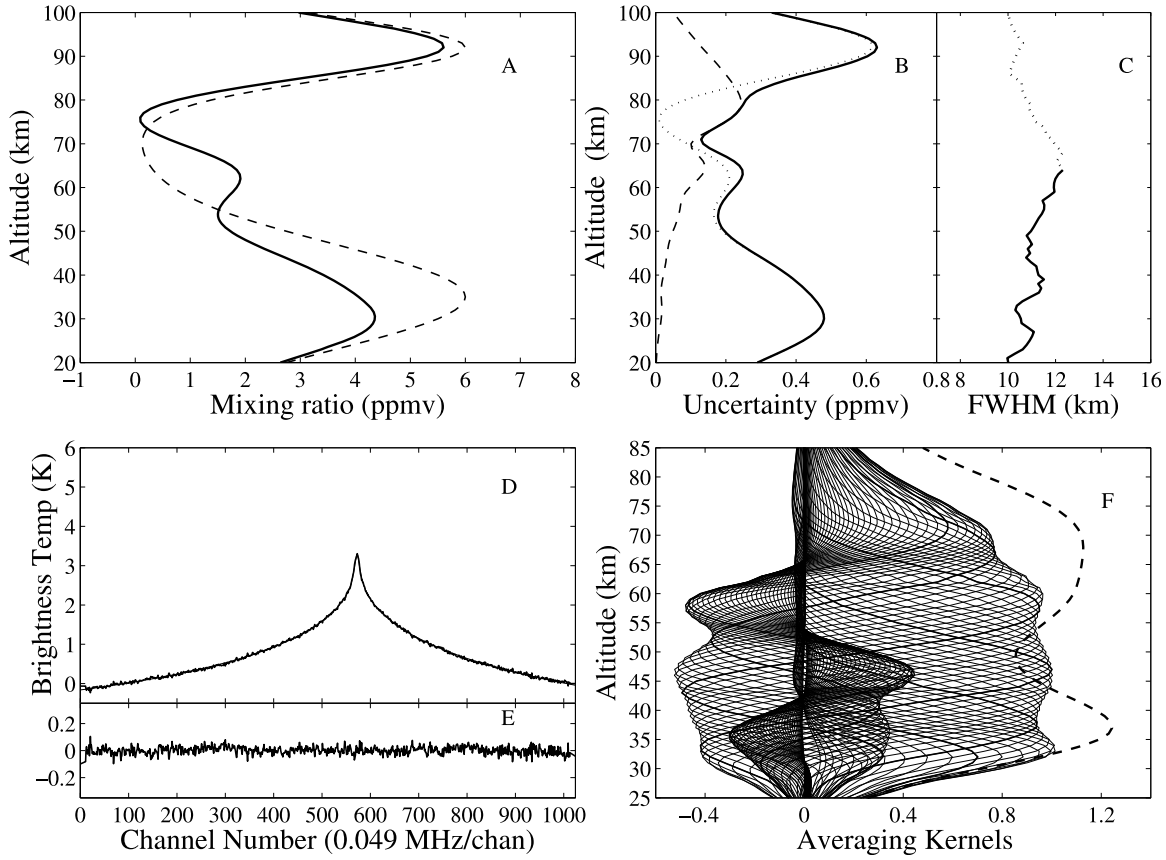

Figure 1. Results from the inversion of a typical GBMS O_3 measurement, carried out on 22 February 2011. (a) The a priori (dashed line) and the retrieved (solid line) profiles. (b) The error estimate, with the dashed line indicating the uncertainty due to spectral noise, the dotted line indicating the 11% uncertainty due to calibration, data scaling procedures, and uncertainties in the forward model parameters, and the solid line being the sum in quadrature of the two errors. (c) An estimation of the retrieval's vertical resolution obtained by calculating the FWHM of the averaging kernels. (d) The spectral measurement and the synthetic spectrum. (e) The residual obtained as the difference synthetic minus measurement spectra. (f) The averaging kernels (solid lines) and the sensitivity parameter (dashed line). The FWHM line in Figure 1c is solid at altitudes where the FWHM is a meaningful representation of the vertical resolution; it is dashed elsewhere. In Figure 1f the AKs corresponding to 30, 40, 50, 60, 70, and 80 km are indicated with a thicker solid line.

to amount to 8% [*Cheng et al.*, 1996; *Parrish et al.*, 1988], whereas the uncertainties related to parameters used in the forward model calculation (e.g., spectroscopic parameters, pressure and temperature vertical profiles) amount to a total of 7%. These two sources of error added in quadrature result in an overall $\pm 1\sigma$ of $\sim$11%. We consider spectroscopic parameters as a source of systematic error, whereas pressure and temperature vertical profiles cause random errors. However, the uncertainties related to the calibration and data scaling can be both systematic and random, most likely systematic in the short term, due to specific weather conditions that last from several days to weeks (e.g., a thermal inversion that affects our estimate of tropospheric emission), but random in the long run (e.g., over multiple field campaigns) [e.g., *Parrish et al.*, 1988]. We will consider these latter uncertainties to be entirely systematic and conservatively assume that all of the GBMS 11% uncertainty is of systematic origin. The contribution of spectral measurement noise to the uncertainty in the retrieved profile has been assessed by means of the OE framework according to *Connor et al.* [1995] [see also *Fiorucci et al.*, 2011]. Finally, the observing technique is characterized by a limited vertical resolution and this is accounted for in the smoothing error. *Rodgers* [2000] and *Connor et al.* [1995], however, warn against the use of the smoothing error when an accurate knowledge of the variability of the true state of the atmosphere in not available. As a result, we do not include it in our error estimate and refer to the GBMS O_3 profiles as a smoothed representation of the true atmospheric O_3 vertical profiles. Furthermore, when comparing data sets with different vertical resolution, the smoothing error can be essentially accounted for by convolving the higher-resolution profile (in our case all the correlative data sets) with the AKs of the lower resolution measurements (those of the GBMS). Generally, the total uncertainty on the GBMS retrieved profiles, determined by adding in quadrature the errors due to the

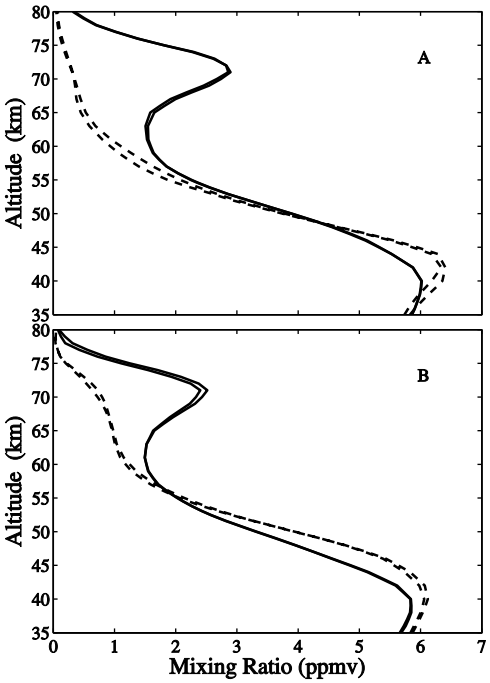

Figure 2. Averages of ROSE O_3 profiles extracted for the (a) SABER-GBMS comparison and the (b) MLS-GBMS comparison. Solid and dashed lines indicate nighttime and daytime profiles, respectively. ROSE averages associated with the GBMS and with SABER data in Figure 2a (or with GBMS and MLS data in Figure 2b) are not drawn differently.

different sources, is given by the larger of 11% or 0.2 ppmv (Figure 1b), with small differences depending on observing conditions.

4. Correlative Data Sets

4.1. Aura MLS

[15] The Earth Observing System (EOS) Microwave Limb Sounder (hereafter indicated simply as MLS) was launched in July 2004 into a Sun-synchronous near-polar orbit aboard the Aura satellite [*Waters et al.*, 2006]. Aura MLS observes many chemical species using five broad spectral regions between 118 GHz and 2.5 THz. The version 3.3 (v3.3) MLS O_3 vertical profiles are obtained from the inversion of measurements in the 240 GHz band. In the stratosphere and above, v3.3 ozone profiles are very similar to the v2.2 profiles which are validated by *Froidevaux et al.* [2008] and are recommended for scientific use only up to 0.02 hPa (~71–73 km altitude), as they start to depend strongly on the a priori profile at lower pressures. Some information, such as average day/night differences, are, however, considered reliable at higher altitudes. The vertical resolution of Aura MLS O_3 profiles degrades from 3 to 5.5 km going from 1 hPa (~45 km altitude) to 0.02 hPa, whereas the horizontal (along track) resolution improves from 450 to 200 km in the same vertical range. The cross-track resolution is fixed at 6 km, and it is due to the MLS field of view at 240 GHz. Table 3.17.1 in the v3.3 MLS data quality document (http://mls.jpl.nasa.gov/data/datadocs.php) shows that MLS O_3 profiles have a single-profile precision of 0.2 ppmv at 1 hPa which degrades to 1.4 ppmv at 0.02 hPa [see also *Froidevaux et al.*, 2008, Table 2]. On the basis of the validation work of *Froidevaux et al.* [2008] and *Boyd et al.* [2007], MLS O_3 v2.2 (and therefore v3.3) upper stratospheric and mesospheric measurements agree within 10% with satellite-based and ground-based measurements.

4.2. TIMED SABER

[16] The Sounding of the Atmosphere using Broadband Emission Radiometry (SABER) instrument is on board the Thermosphere Ionosphere Mesosphere Energetics and Dynamics (TIMED) satellite which was launched in December 2001 into a Sun-synchronous circular orbit with an inclination of 74.1° [*Russell et al.*, 1999]. SABER provides global observations of several chemical species and measures ozone profiles from 15 to 100 km by limb scanning the atmosphere at 1.27 μm and 9.6 μm. SABER has an along-track resolution of 375 km (but less than 100 km for the altitude range of interest here) and a vertical resolution better than 2 km. Version 1.07 O3 measurements have a precision of 1%–2% in the stratosphere and 3%–5% in the lower mesosphere. *Rong et al.* [2009] compared SABER O3 with several correlative data sets (e.g., SBUV/2, MIPAS, MLS, and SAGE II) and results show that SABER O3 is biased high from the middle stratosphere to the lower mesosphere in all comparisons. During nighttime at high northern latitudes (50°–90°N), this high bias ranges from 10 to 25% going from 35 to 60 km altitude and then decreases to 15% at 70 km with respect to MIPAS [see *Rong et al.*, 2009, Figure 12]. In an analogous comparison with MLS O_3 [*Rong et al.*, 2009, Figure 15], SABER O_3 is biased high by 10%–20% in the altitude range from 35 to 55 km but shows a good agreement (within 5%) at 70 km. *Smith et al.* [2008] compare nighttime SABER and GOMOS O_3 and find SABER high biased by ~25% at 75 km altitude but in good agreement with GOMOS at 80 km, where the O_3 minimum is located. Finally, all the comparisons reported by *Rong et al.* [2009] indicate that SABER describes the lower mesospheric O_3 diurnal variability very well.

4.3. ROSE

[17] ROSE is a global three-dimensional mechanistic model simulating dynamics and chemistry in the middle atmosphere. The current 2004 version is an evolution of the original model developed by Klaus Rose and Guy Brasseur [*Smith and Marsh*, 2005, and references therein]. ROSE solves for the concentrations of 29 chemical species over a fixed grid spaced 5° in latitude and 11.25° in longitude. It covers pressure levels from 90 hPa to 5×10^{-5} hPa (~17–188 km altitude), with ~2.5 km of vertical resolution. ROSE computes concentrations of chemical species taking into account a total of 118 gas-phase, heterogeneous, and photolysis reactions with a time step of 7.5 min. Almost all of the reaction rate coefficients are taken from a JPL catalog [*Sander et al.*, 2003]. The ROSE grid points that surround Thule are 77.5°N, 67.5°W; 77.5°N, 78.75°W; 72.5°N, 67.5°W; and 72.5°N, 78.75°W.

5. Intercomparisons' Criteria

[18] The GBMS measures only one chemical species at a time and its spectral passband must be tuned to a different

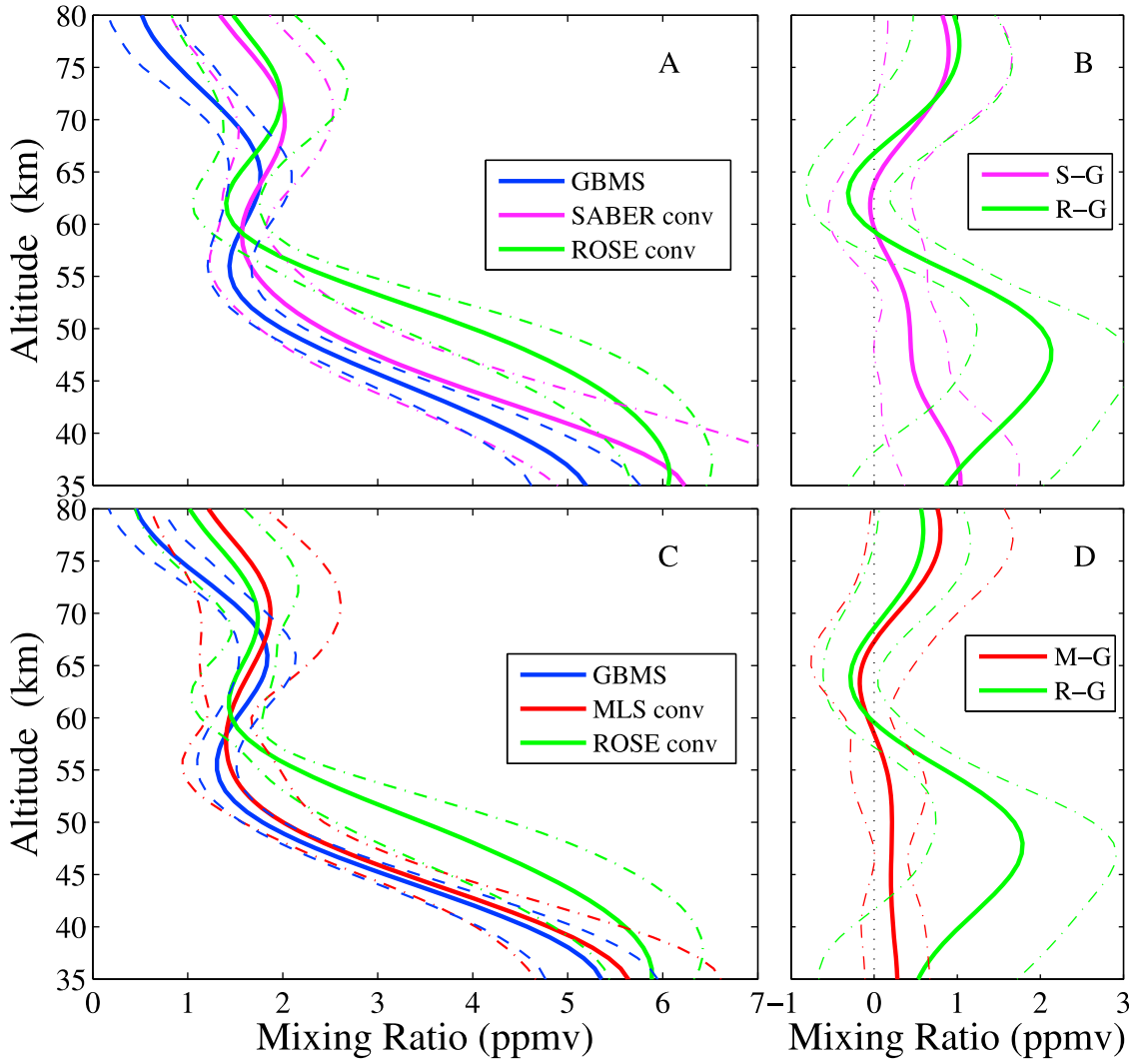

Figure 3. (a, c) Nighttime O_3 mean profiles of GBMS (blue solid lines), convolved MLS (red solid line, Figure 3c), convolved SABER (magenta solid line, Figure 3a), and convolved ROSE coincident with GBMS measurements (green solid line, Figures 3a and 3c). Dashed blue lines (Figures 3a and 3c) depict the GBMS O_3 uncertainty shown in Figure 1b, whereas the dash-dotted red, magenta, and green lines depict the ± 1 standard deviation of the mean of MLS, SABER, and ROSE, respectively. (b, d) The corresponding absolute differences between the mean values shown in Figures 3a and 3c. Solid lines indicate the differences (red for MLS-GBMS, green for ROSE-GBMS, and magenta for SABER-GBMS) with the corresponding ± 1 standard deviation of the mean differences indicated with dash-dotted lines.

frequency each time a different chemical species is to be observed. As GBMS operations are aimed at daily observations of four species (O_3, CO, HNO_3, and N_2O), the time devoted to each species is limited and coincidences with satellite observations can be sparse. Generally, O_3 is observed twice daily, one time at around noon and a second time during nighttime, for a total of 4–6 h of integration. Since GBMS winter campaigns last for approximately 6 weeks, and each winter there have always been about 7–10 days of poor weather and/or instrumental malfunctioning, we can count on a total of 178 O_3 profiles over the three years.

[19] We compare GBMS O_3 profiles with concurrent MLS, SABER, and ROSE profiles, convolved using the GBMS averaging kernels to account for the lower vertical resolution of GBMS measurements. The MLS-GBMS and SABER-GBMS matches are independent from one another and occur largely on different dates. Generally, comparisons during transition times between night and day were avoided by observing the evolution of GBMS 15 min spectra and the time evolution of ROSE profiles at the closest grid point to the GBMS observations. If any of the two data sets presented significant variations within ± 1 h we did not take the correspondent GBMS measurement into consideration for the comparison. In what follows, as the selection process applied to MLS and SABER data is analogous, we will generically refer to both of them as "satellite."

[20] We first selected the satellite/GBMS coincidences and then, for each match, extracted the two ROSE profiles on grid points the closest (in space and time) to the satellite

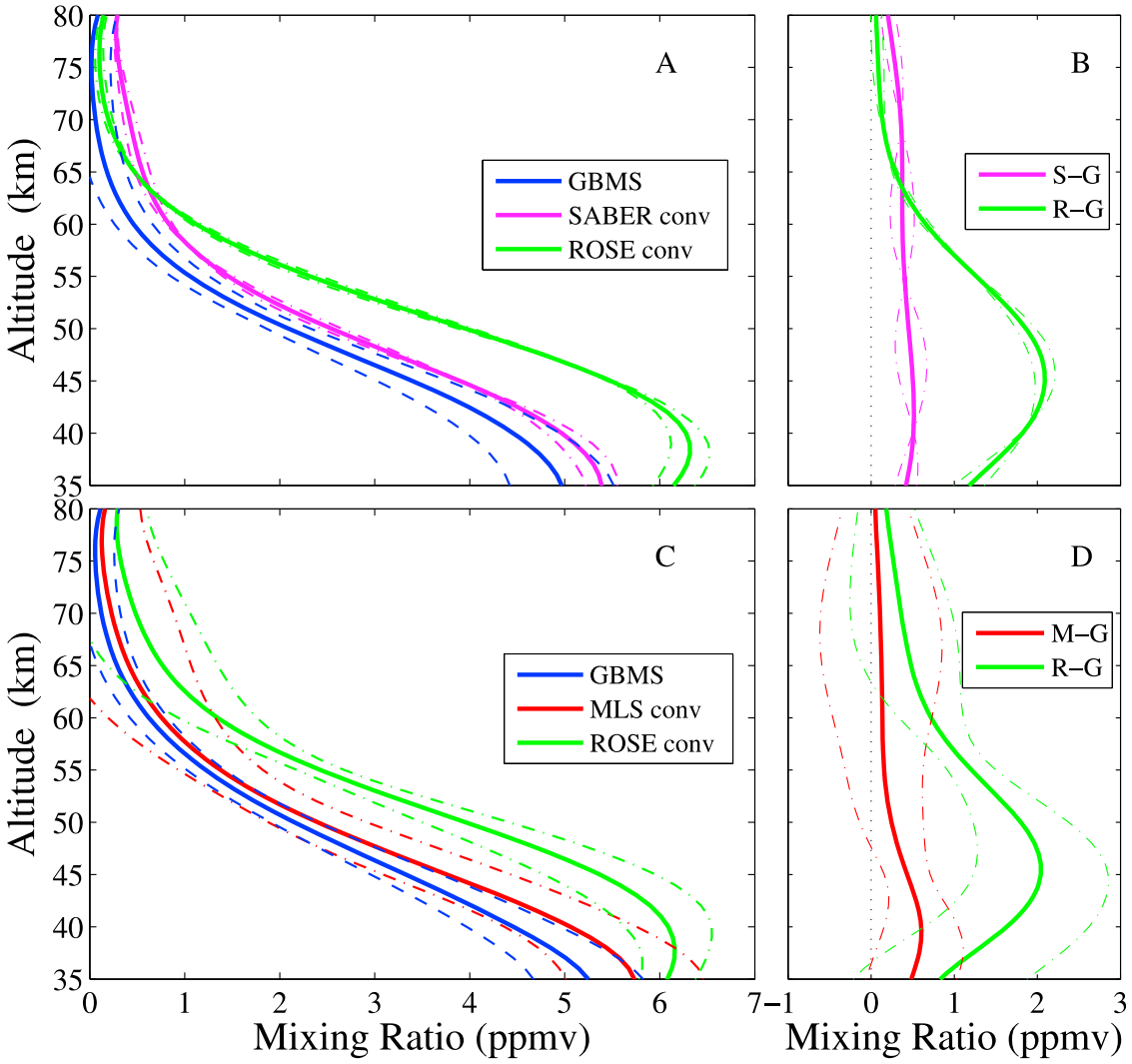

Figure 4. Same as Figure 3 but for daytime profiles. The SABER mean profile (Figure 4a) and corresponding SABER-GBMS difference (Figure 4b) should be approached with caution, being an average of only two coincidences.

profile and to the GBMS mesospheric observations. In general, although each pair of satellite and GBMS profiles used in the comparison meets our coincidence criteria, they are often the closest to different ROSE grid points. Similarly, if the satellite passage is one hour away from the starting time of a GBMS integration, the two corresponding profiles have their best temporal match with ROSE profiles at different times. For this reason, for each pair of matching satellite and GBMS profiles we have a pair of ROSE profiles, one being the closest in time and space to the GBMS profile and the other one to the satellite profile. As an additional check aimed at making sure that comparisons were not affected by O_3 diurnal changes, we intercompared the two ROSE profiles and verified that their differences were smaller than 0.5 ppmv (see also the standard deviation of the ROSE mean profiles depicted in Figures 3 and 4). If this was not the case, the satellite/GBMS coincidence data point was discarded. Our coincidence criteria between GBMS and satellite data are $\pm 2^\circ$ latitude, $\pm 10^\circ$ longitude (and maximum distance of 300 km), and ± 1 h. For matching GBMS and ROSE, as well as satellite and ROSE, the spatial requirements are the same but the time requirement is narrowed down to ± 0.5 h. The use of two separate sets of ROSE profiles for each comparison (MLS-GBMS and SABER-GBMS), one associated with the GBMS data and the other associated to the satellite data under consideration, provide us with an independent evaluation of the validity of the chosen coincidence criteria. In order to clarify this aspect, Figure 2 shows averages of all the ROSE profiles used in the intercomparisons (divided into GBMS daytime matches, GBMS nighttime matches, satellite daytime matches, and satellite nighttime matches). In Figure 2a, the nighttime averages (solid lines) and daytime averages (dashed lines) of ROSE profiles extracted in coincidence with GBMS measurements and with SABER retrieved ozone using the 9.6 μm measurements are depicted. Similarly, in Figure 2b we report averages of ROSE profiles that are coincident with MLS measurements. Each pair of nighttime and daytime profiles match each other very closely and we did not mark differently

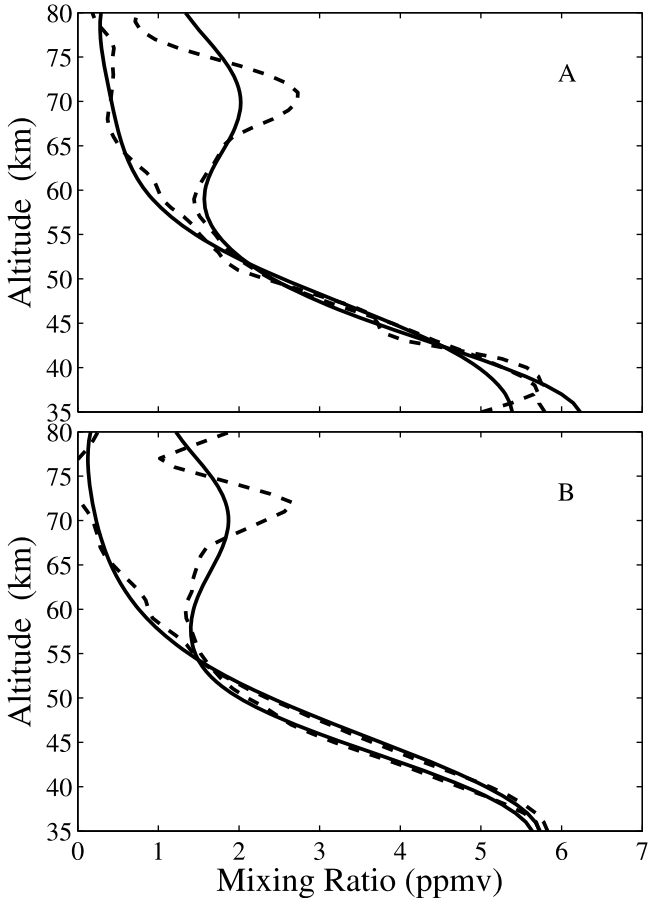

Figure 5. (a) SABER original/higher-resolution (dashed lines) and convolved (solid lines) averaged nighttime and daytime profiles. (b) Analogous profiles for MLS.

the two averages matching GBMS from those matching MLS or SABER O_3.

[21] All the selected GBMS profiles were separated in two groups: apparent daytime and apparent nighttime profiles. We specify "apparent" because in this context we are not interested in showing the relationship between Sun exposure and O_3 concentration, but we only aim at evaluating systematic differences among the 4 data sets that may be found in the two different cases encountered: typical daytime and typical nighttime profiles. In fact, given the peculiar location and exposure to sunlight of air masses passing over Thule, owing to the high latitude of the site, to the season when the field campaigns occurred, and to the active dynamics typical of the winter Arctic middle/upper atmosphere, a straightforward separation of the two cases simply based on solar zenith angles would not suffice. GBMS vertical profiles considered apparent daytime profiles are those with values always below 1 ppmv between 60 and 80 km altitude, that is, those profiles which do not present any sign of a tertiary ozone peak. All the remaining selected GBMS profiles are apparent nighttime profiles and display a tertiary ozone vmr peak larger than 1 ppmv between 60 and 80 km altitude. Ultimately, the comparison with MLS can count on a total of 34 GBMS profiles, 17 representative of the daytime and 17 representative of nighttime conditions. For the comparison between GBMS and SABER, a total of 20 coincidences are obtained, 18 during nighttime and only 2 coincidences during daytime. Given the extremely small number of daytime matches with SABER, these specific comparisons should be approached with caution.

6. Discussion

6.1. Data Intercomparisons

[22] In Figures 3a and 3c the averages of nighttime profiles of all the intercompared data sets are shown (see Figure 3 caption for details). The averages of the three correlative data sets are obtained by averaging the original/higher-resolution profiles after having convolved each profile using the averaging kernels of the matching GBMS profile. From the ROSE data set only the averages of profiles matching the GBMS observations are represented, as Figure 2 already showed that they are consistent with ROSE averages matching satellite data. It is worth stressing that the ± 1 standard deviations of the mean of MLS, SABER, and ROSE profiles (dash-dotted lines in Figures 3a and 3c) include the natural variability of the atmosphere and are not an indication of the precision of the three data sets. O_3 natural variability can be particularly large in the stratosphere where the position and strength of the polar vortex (unaccounted for in the selection process leading to the averaged profiles of Figures 3a and 3c) greatly affect the O_3 concentration observed above Thule. Figures 3b and 3d illustrate the absolute differences between the convolved correlative data sets and GBMS O_3, with dash-dotted lines indicating ± 1 standard deviation of the mean difference. Figure 4 is analogous to Figure 3 but for daytime profiles. In order to illustrate the effect of convolving satellite and model profiles with GBMS averaging kernels, in Figures 5a and 5b both the averages of the higher-resolution profiles (dashed lines) and the averages of the convolved profiles (solid lines) of SABER (Figure 5a) and MLS (Figure 5b) are shown. From comparing the higher resolution and the convolved averages in Figure 5 we gain confidence in the capability of the GBMS averaging kernels to resolve the ozone tertiary maximum, even though a "formal" GBMS vertical resolution larger than 12 km at 70 km altitude (see Figure 1c) might have suggested otherwise.

[23] The intercomparison results reported in Figures 3 and 4 suggest that the ROSE model is, on average, biased high from the middle stratosphere to the stratopause in the northern high latitudes during winter. This appears to be true with respect to all the other data sets discussed here. With respect to GBMS O_3, this averaged bias reaches a maximum value of $\sim$2 ppmv at 45 km altitude (Figures 3 and 4) and it is evident in the altitude range above the region where heterogeneous reactions take place (i.e., above $\sim$30 km) and below the atmospheric levels where O_3 diurnal variations start to be significant. This suggests that the stratospheric dynamics in ROSE might be the reason for this high bias (see later for further discussion).

[24] MLS and GBMS O_3 profiles agree well from 35 to 65 km (Figures 3c and 4c), with the GBMS being in most cases lower than MLS. Overall, the GBMS O_3 low bias amounts to $\sim$9% when averaged in the 35–65 km altitude range. The agreement is good also in the daytime mesosphere (Figure 4d), where the difference is small and well within GBMS uncertainties. The GBMS and SABER

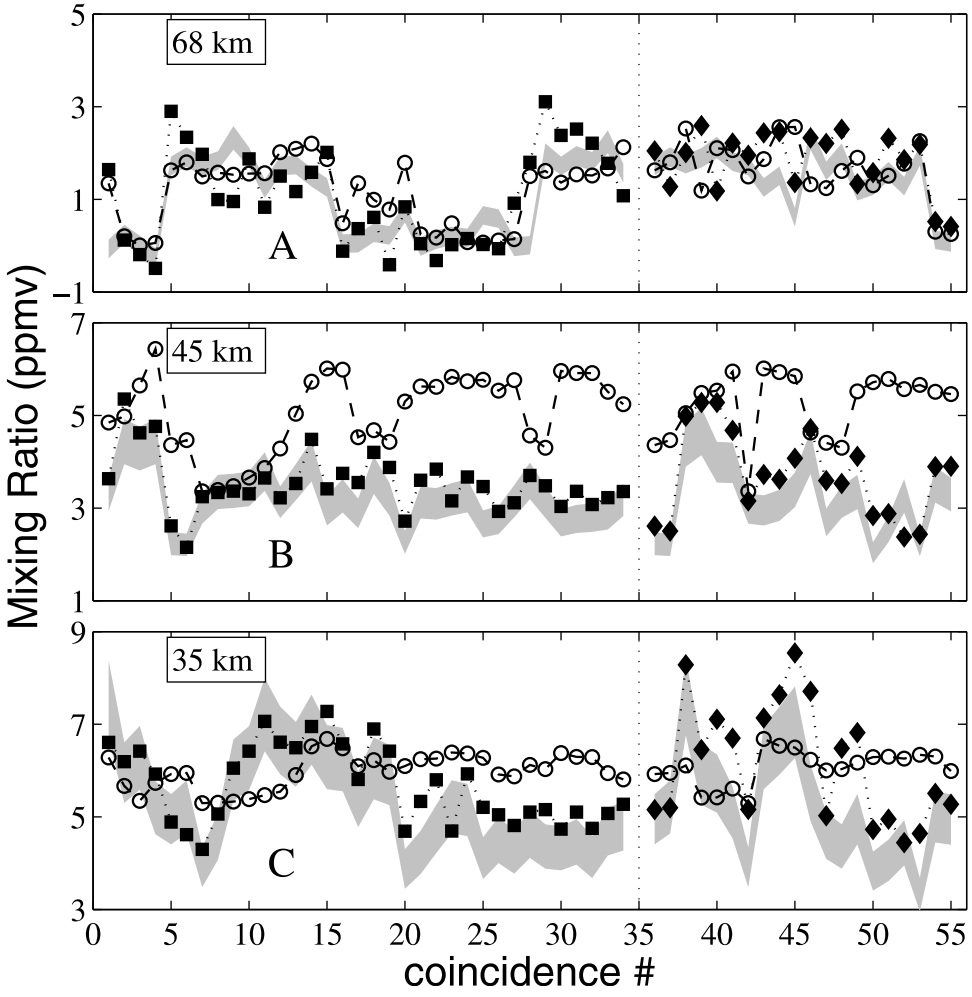

Figure 6. Series of all the matching data points from the four data sets at three critical altitudes: (a) 68 km, (b) 45 km, and (c) 35 km. Coincidences among GBMS (gray area covering $O_3 \pm 1\sigma$), MLS (solid squares), and ROSE (open circles) O_3 are arbitrarily displayed with a coincidence number from 1 to 34; matches of GBMS, SABER (solid diamonds), and ROSE O_3 are displayed with a coincidence number from 36 to 55. The only two daytime GBMS-SABER matches are coincidences 54 and 55.

nighttime O_3 profiles below 60 km altitude differ by a larger amount than the MLS - GBMS difference (compare Figures 3b and 3d). We recall, however, that SABER O_3 is known to be biased high by 10%–20% in the altitude range from 35 to 55 km (see section 4.2) and this accounts for the difference observed with respect to the GBMS.

[25] In the nighttime mesosphere (Figures 3a and 3c), GBMS retrievals indicate the regular formation of the tertiary ozone maximum, even though it was not included, on purpose, in the O_3 vmr a priori profile (Figure 1a). The tertiary ozone peak from all the data sets plotted in Figure 3 is estimated to be between 1.7 and 2 ppmv, with GBMS measurements displacing its altitude downward by 4–5 km with respect to all other data sets. This results in the GBMS O_3 values being biased low with respect to the correlative data sets in the 70–80 km altitude range by a quantity that increases with altitude and tops at 0.8 ppmv near 80 km.

[26] In order to further discuss some of the results found in Figures 3 and 4, in Figure 6 we show all the available O_3 vmr values at the three most interesting altitude levels for the comparison GBMS/MLS/ROSE (34 matches) and the comparison GBMS/SABER/ROSE (20 matches). As the coincidences found are scattered over three winter campaigns, it would be meaningless to display these values versus time, and in Figure 6 we simply numbered the GBMS versus MLS coincidences from 1 to 34 and the GBMS versus SABER coincidences from 36 to 55, separating the two sets with a dotted vertical line (at #35). The GBMS O_3 values are represented with a gray band which accounts for GBMS O_3 vmr $\pm 1\sigma$ (11% or 0.2 ppmv), ROSE values are depicted with empty circles, MLS and SABER values are represented with solid squares and diamonds, respectively. In Figure 6c (35 km altitude) we notice that ROSE values are rather steady and do not follow the variations displayed by the other three data sets. This behavior is confirmed in Figures 3b and 3d and Figures 4b and 4d, where, although the difference at 35 km between ROSE and GBMS O_3 is comparable to the MLS-GBMS and SABER-GBMS differences, the 1σ of the ROSE-GBMS difference is significantly larger than those found in the MLS versus GBMS and SABER versus GBMS O_3 comparisons. We attribute this result to the dynamics in the ROSE model which may not

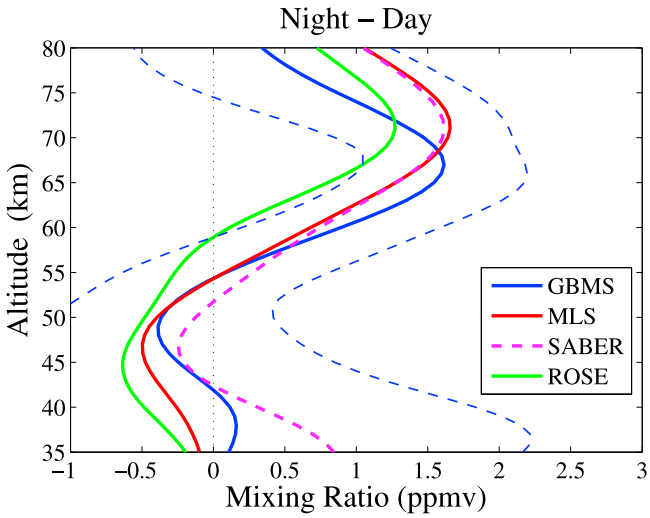

Figure 7. Profiles of night minus day average differences for each data set. GBMS, MLS, and ROSE diurnal O_3 differences are indicated with solid lines: GBMS in blue, MLS in red, and ROSE in green. SABER (to be considered with caution since it uses the daytime mean calculated using only two profiles) is indicated with a magenta dashed line. GBMS and ROSE profiles included in the night minus day averages are only those matching MLS data. The night minus day profiles of the correlative data sets are obtained from the averages of convolved data. Only the ± 1 standard deviation of the GBMS mean night minus day difference is depicted (using blue dashed lines) for clarity.

match the extremely high activity that characterizes the Arctic winter middle atmosphere. Figure 6b (45 km altitude) shows a different picture, with ROSE O_3 values largely variable but systematically larger than values from the other three data sets (see also Figures 3 and 4). In winter, middle atmospheric ozone forms essentially at lower latitudes and is then transported to the Arctic region. This suggests that the observed discrepancies at 45 km could be due to problems with the mean circulation in the ROSE model, where the poleward component of the circulation around 40–55 km may be too strong or the downward component at around the same altitudes too weak.

[27] Figure 6 shows that GBMS O_3 measurements at all levels are very well correlated with both satellite data sets. At 68 km (Figure 6a), where photochemistry plays a key role in determining O_3 concentrations, O_3 modeled values from ROSE are very well correlated with the measurements.

6.2. Mesospheric O_3 Diurnal Variation

[28] In Figure 7, the difference between the convolved nighttime and daytime profiles is shown. Solid lines represent the GBMS (blue), MLS (red), and ROSE (green) O_3 night minus day differences, the dashed magenta line represents the corresponding SABER difference, and the dashed thin blue lines indicate the $\pm 1\sigma$ of the GBMS difference profile (for clarity we omitted all the others) calculated as the sum of the standard deviations of the mean nighttime and daytime GBMS profiles. The SABER profile should be approached with caution as it relies on the daytime average which is based only on 2 coincidences with GBMS. For the same reason, and in order to consistently compare GBMS, MLS, and ROSE results, GBMS and ROSE profiles that went into the averages of Figure 7 are only those matching MLS data. However, including profiles matching SABER measurements to the GBMS and ROSE nighttime and daytime averages would have a small impact on the average differences shown in Figure 7. Figure 7 shows that all four data sets agree well on the average night to day variation of mesospheric O_3, with GBMS, MLS, and SABER measurements displaying the same peak magnitude of $\sim$1.6 ppmv. Being closely related to the formation of the ozone tertiary maximum (see Figures 3a and 3c), also the GBMS diurnal variation profile shows a peak height 4 km below those determined by the other data sets (at 67 km altitude compared to the 71 km of MLS, SABER, and ROSE).

[29] Once it has been established the capability of GBMS measurements to detect the peak of diurnal ozone variations without any a priori knowledge of the tertiary ozone maximum (see the a priori profile in Figure 1a), it is useful to evaluate the improvements that a more realistic a priori O_3 vmr vertical profile (i.e., one that characterizes at best the atmospheric state) could bring to GBMS estimates of the mesospheric diurnal variations. For this purpose, nighttime GBMS spectra have also been inverted using an a priori identical to that shown in Figure 1a except for the addition of an O_3 vmr Gaussian profile centered at 71 km altitude and with a peak of 1.5 ppmv. The altitude of this peak was inferred from the average (not convolved) MLS and SABER O_3 nighttime profiles and from the literature [*Marsh et al.*, 2001; *Hartogh et al.*, 2004]. The obtained GBMS O_3 diurnal variation profile is shown in Figure 8 with a thick solid blue line, whereas the profile obtained in the previous analysis (the one of Figure 7) is indicated with a thin solid

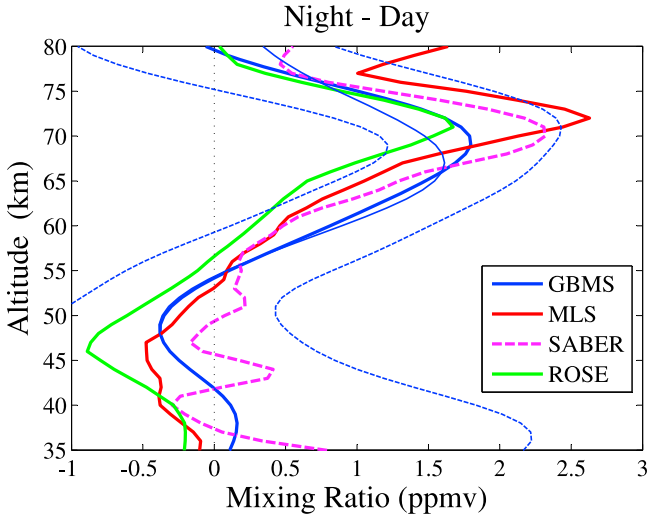

Figure 8. Similar to Figure 7 but the GBMS O_3 difference is now calculated from nighttime GBMS O_3 vmr vertical profiles obtained using a more realistic a priori (see text). Additionally, the night minus day profiles of MLS, SABER, and ROSE are calculated from averages of the original/higher-resolution (not convolved) data. The GBMS diurnal difference of Figure 7 is also indicated with a thin solid blue line.

blue line. The original/higher-resolution MLS, SABER, and ROSE diurnal O_3 difference profiles are also depicted in Figure 8. The new GBMS diurnal variation profile peaks at 69 km altitude with a difference night minus day of 1.8 $\pm$ 0.6 ppmv. This result resembles closely the higher-resolution diurnal variation profiles of the two satellite data sets, considered in this case (MLS in particular) a good representation of the true state of the atmosphere. In fact, MLS and SABER night minus day values are enclosed within the GBMS upper standard deviation curve (rightmost dashed blue line in Figure 8) at nearly all mesospheric altitudes. This suggests that, if a valid description of the atmospheric state is adopted in the O_3 vmr a priori profile, the daily evolution of the tertiary ozone peak is very well captured by the GBMS both in size and altitude.

7. Summary

[30] The GBMS was setup at the NDACC Arctic station located at Thule Air Base, Greenland, in January 2009 and has accomplished three winter campaigns of several stratospheric and mesospheric trace gas measurements since then. Concurrently, the retrieval algorithm adopted for inverting the GBMS spectral measurements has been changed and is now an adaptation of the optimal estimation method which is the most widely used technique within the atmospheric microwave remote sensing community in general and the NDACC microwave groups in particular. In this work we examined the GBMS O_3 retrievals from 35 to 80 km altitude obtained by using only one of the two GBMS back-end spectrometers, the narrowband AOS (50 MHz passband, 65 kHz resolution). We will discuss the retrievals obtained using the wideband AOS (vertical profiles from 15 to 45 km) in a future publication.

[31] The GBMS retrievals shown in Figure 1 were characterized in section 3 that described their uncertainty, their vertical resolution and sensitivity, and showed the remarkable quality of the spectral measurements. We then proceeded with comparing the GBMS O_3 profiles with MLS, SABER and ROSE O_3 colocated profiles, introducing these correlative data sets and discussing the criteria adopted for selecting their vertical profiles in sections 4 and 5, respectively.

[32] Figures 3, 4, and 6 show the results of these intercomparisons. The GBMS agrees well with MLS measurements in the stratosphere and lower mesosphere. It displays a negative bias which is within the GBMS uncertainties at all altitudes and amounts to $\sim$9% when averaged over altitudes below 65 km. An apparent larger difference is found between GBMS and SABER O_3 profiles. The agreement between the two data sets is however comparable to or better than the agreement between GBMS and MLS once the results take into consideration the known 10%–20% high bias of SABER stratospheric and lower mesospheric O_3 profiles [*Rong et al.*, 2009; *Smith et al.*, 2008]. Figure 6 shows that GBMS O_3 values at three key altitudes are very well correlated with MLS and SABER results, whereas ROSE O_3 values suggest that the dynamics implemented in the model may need tuning.

[33] In the nighttime mesosphere, GBMS measurements proved to be capable of detecting the ozone tertiary maximum without any forcing from the O_3 vmr a priori profile. All the smoothed data sets find the magnitude of the tertiary ozone peak to be between 1.7 and 2 ppmv, with GBMS measurements locating it at a lower altitude with respect to the other data sets by 4–5 km. Similarly, GBMS, MLS, and SABER O_3 nighttime minus daytime average profiles (Figure 7) show a diurnal variation peak value of $\sim$1.6 ppmv, with the GBMS peak altitude shifted downward by 4 km. If the a priori information for the analysis of GBMS spectra is improved to better describe the atmospheric state at night, and therefore a small tertiary maximum is added to the O_3 vmr a priori profile, the reanalyzed ground-based data produces a diurnal variation profile (Figure 8) with a peak of 1.8 $\pm$ 0.6 ppmv located only 1 or 2 km below the altitude indicated by the higher-resolution satellite-based measurements.

[34] This intercomparison work indicates that the GBMS O_3 retrievals and the GBMS measurements of the diurnal variation of mesospheric O_3 at the high northern latitudes of Thule are a valid contribution to the NDACC database and a valuable asset for validating numerical models and satellite-based measurements.

[35] **Acknowledgments.** This material is based on work also supported by the National Science Foundation under grant 0936365. G. Muscari is indebted to Bob de Zafra for designing, building, and upgrading the GBMS, as well as for the economic and technical support that led to many successful GBMS field campaigns. We thank Pietro Paolo Bertagnolio, Svend Erik Ascanius, Claudia Di Biagio, and Giorgio di Sarra for their technical assistance during the GBMS field campaigns at Thule. We also thank three reviewers for their useful comments on the original manuscript. The National Center for Atmospheric Research is sponsored by the National Science Foundation. Work at the Jet Propulsion Laboratory, California Institute of Technology, was done under contract with NASA.

References

Boyd, I. S., A. D. Parrish, L. Froidevaux, T. von Clarmann, E. Kyrölä, J. M. Russell III, and J. M. Zawodny (2007), Ground-based microwave ozone radiometer measurements compared with Aura-MLS v2.2 and other instruments at two Network for Detection of Atmospheric Composition Change sites, *J. Geophys. Res.*, *112*, D24S33, doi:10.1029/2007JD008720.

Brasseur, G., and S. Solomon (2005), *Aeronomy of the Middle Atmosphere: Chemistry and Physics of the Stratosphere and Mesosphere*, 3rd ed., Springer, Dordrecht, Netherlands.

Cheng, D., R. L. de Zafra, and C. Trimble (1996), Millimeter wave spectroscopic measurements over the South Pole: 2. An 11-month cycle of stratospheric ozone observations during 1993–1994, *J. Geophys. Res.*, *101*, 6781–6793, doi:10.1029/95JD03652.

Coe, H., B. J. Allan, and J. M. C. Plane (2002), Retrieval of vertical profiles of NO_3 from zenith sky measurements using an optimal estimation method, *J. Geophys. Res.*, *107*(D21), 4587, doi:10.1029/2002JD002111.

Connor, B. J., A. Parrish, J. J. Tsou, and M. P. McCormick (1995), Error analysis for the ground-based microwave ozone measurements during STOIC, *J. Geophys. Res.*, *100*, 9283–9291, doi:10.1029/94JD00413.

de Zafra, R. L. (1995), The ground-based measurements of stratospheric trace gases using quantitative millimeter wave emission spectroscopy, in *Diagnostic Tools in Atmospheric Physics: Proceedings of the International School of Physics "Enrico Fermi"*, pp. 23–54, Soc. Ital. Fis., Bologna, Italy.

de Zafra, R. L., V. Chan, S. Crewell, C. Trimble, and J. M. Reeves (1997), Millimeter wave spectroscopic measurements over the South Pole: 3. The behavior of stratospheric nitric acid through polar fall, winter, and spring, *J. Geophys. Res.*, *102*, 1399–1410, doi:10.1029/95JD03679.

Di Biagio, C., G. Muscari, A. di Sarra, R. L. de Zafra, P. Eriksen, I. Fiorucci, and D. Fuà (2010), Evolution of temperature, O_3, CO, and N_2O profiles during the exceptional 2009 Arctic major stratospheric warming as observed by lidar and millimeter-wave spectroscopy at Thule (76.5°N, 68.8°W), Greenland, *J. Geophys. Res.*, *115*, D24315, doi:10.1029/2010JD014070.

Fiorucci, I., et al. (2008), Measurements of low amounts of precipitable water vapor by millimeter wave spectroscopy: An intercomparison with

radiosonde, Raman lidar, and Fourier transform infrared data, *J. Geophys. Res.*, *113*, D14314, doi:10.1029/2008JD009831.

Fiorucci, I., G. Muscari, and R. L. de Zafra (2011), Revising the retrieval technique of a long-term stratospheric HNO_3 data set: From a constrained matrix inversion to the optimal estimation algorithm, *Ann. Geophys.*, *29*, 1317–1330, doi:10.5194/angeo-29-1317-2011.

Froidevaux, L., et al. (1996), Validation of UARS Microwave Limb Sounder ozone measurements, *J. Geophys. Res.*, *101*, 10,017–10,060, doi:10.1029/95JD02325.

Froidevaux, L., et al. (2008), Validation of Aura Microwave Limb Sounder stratospheric ozone measurements, *J. Geophys. Res.*, *113*, D15S20, doi:10.1029/2007JD008771.

Hartogh, P., C. Jarchow, G. R. Sonnemann, and M. Grygalashvyly (2004), On the spatiotemporal behavior of ozone within the mesosphere/mesopause region under nearly polar night conditions, *J. Geophys. Res.*, *109*, D18303, doi:10.1029/2004JD004576.

Marsh, D., A. Smith, G. Brasseur, M. Kaufmann, and K. Grossmann (2001), The existence of a tertiary ozone maximum in the high-latitude middle mesosphere, *Geophys. Res. Lett.*, *28*, 4531–4534, doi:10.1029/2001GL013791.

Muscari, G., A. G. di Sarra, R. L. de Zafra, F. Lucci, F. Baordo, F. Angelini, and G. Fiocco (2007), Middle atmospheric O_3, CO, N_2O, HNO_3, and temperature profiles during the warm Arctic winter 2001–2002, *J. Geophys. Res.*, *112*, D14304, doi:10.1029/2006JD007849.

Nedoluha, G., R. Bevilacqua, R. Gomez, D. Thacker, W. Waltman, and T. Pauls (1995), Ground-based measurements of water vapor in the middle atmosphere, *J. Geophys. Res.*, *100*, 2927–2939, doi:10.1029/94JD02952.

Parrish, A., R. L. de Zafra, P. M. Solomon, and J. W. Barrett (1988), A ground-based technique for millimeter wave spectroscopic observations of stratospheric trace constituents, *Radio Sci.*, *23*, 106–118, doi:10.1029/RS023i002p00106.

Parrish, A., B. J. Connor, J. J. Tsou, I. S. Mc Dermid, and W. P. Chu (1992), Ground-based microwave monitoring of stratospheric ozone, *J. Geophys. Res.*, *97*, 2541–2546, doi:10.1029/91JD02914.

Pickett, H. M., R. L. Poynter, E. A. Cohen, M. L. Delitsky, J. C. Pearson, and H. S. P. Müller (1998), Submillimeter, millimeter, and microwave spectral line catalog, *J. Quant. Spectrosc. Radiat. Transfer*, *60*, 883–890, doi:10.1016/S0022-4073(98)00091-0.

Rodgers, C. D. (1976), Retrieval of atmospheric temperature and composition from remote measurements of thermal radiation, *Rev. Geophys.*, *14*, 609–624, doi:10.1029/RG014i004p00609.

Rodgers, C. D. (2000), *Inverse Method for Atmospheric Sounding, Ser. Atmos. Oceanic Planet. Phys.*, vol. 2, World Sci., Singapore.

Rong, P. P., J. M. Russell III, M. G. Mlynczak, E. E. Remsberg, B. T. Marshall, L. L. Gordley, and M. Lopez-Puertas (2009), Validation of Thermosphere Ionosphere Mesosphere Energetics and Dynamics/Sounding of the Atmosphere using Broadband Emission Radiometry (TIMED/SABER) v1.07 ozone at 9.6 μm in altitude range 15–70 km, *J. Geophys. Res.*, *114*, D04306, doi:10.1029/2008JD010073.

Rothman, L. S., et al. (2009), The HITRAN 2008 molecular spectroscopic database, *J. Quant. Spectrosc. Radiat. Transfer*, *110*, 533–572, doi:10.1016/j.jqsrt.2009.02.013.

Russell, J. M., III, M. G. Mlynczak, L. L. Gordley, J. J. Tansock, and R. W. Esplin (1999), Overview of the SABER experiment and preliminary calibration results, *Proc. SPIE Int. Soc. Opt. Eng.*, *3756*, 277–288.

Sander, S. P., et al. (2003), Chemical kinetics and photochemical data for use in stratospheric modeling: Evaluation number 14, *JPL Publ.*, *02–25*, 334 pp.

Smith, A. K., and D. R. Marsh (2005), Processes that account for the ozone maximum at the mesopause, *J. Geophys. Res.*, *110*, D23305, doi:10.1029/2005JD006298.

Smith, A. K., D. R. Marsh, J. M. Russell III, M. G. Mlynczak, F. J. Martin-Torres, and E. Kyrölä (2008), Satellite observations of high nighttime ozone at the equatorial mesopause, *J. Geophys. Res.*, *113*, D17312, doi:10.1029/2008JD010066.

Twomey, S. (1977), *Introduction to the Mathematics of Inversion in Remote Sensing and Indirect Measurements, Dev. Geomath.*, vol. 3, Elsevier Sci., New York.

Waters, J. W., et al. (2006), The Earth Observing System Microwave Limb Sounder (EOS MLS) on the Aura Satellite, *IEEE Trans. Geosci. Remote Sens.*, *44*, 1075–1092, doi:10.1109/TGRS.2006.873771.

C. Cesaroni, I. Fiorucci, and G. Muscari, Istituto Nazionale di Geofisica e Vulcanologia, sez. Roma 2, Via di Vigna Murata 605, I-00143 Rome, Italy. (giovanni.muscari@ingv.it)

L. Froidevaux, Jet Propulsion Laboratory, California Institute of Technology, Pasadena, CA 91109, USA.

M. G. Mlynczak, NASA Langley Research Center, Hampton, VA 23681, USA.

A. K. Smith, Atmospheric Chemistry Division, National Center for Atmospheric Research, Boulder, CO 80305, USA.